Structural and elastic characterization of Cu-implanted SiO_2 films on Si(100) substrates

J. Shirokoff
Faculty of Engineering and Applied Science, Memorial University of Newfoundland, St. John's, Newfoundland and Labrador A1B 3X5, Canada

C. K. Young, L. C. Brits, and G. T. Andrews[a)]
Department of Physics and Physical Oceanography, Memorial University of Newfoundland, St. John's, Newfoundland and Labrador A1B 3X7, Canada

B. Johannessen and M. C. Ridgway
Department of Electronic Materials Engineering, Australian National University, Research School of Physical Science and Engineering, Canberra ACT 0200 Australia

(Received 7 July 2006; accepted 20 December 2006; published online 16 February 2007)

Cu-implanted SiO_2 films on Si(100) have been studied and compared to unimplanted SiO_2 on Si(100) using x-ray methods, transmission electron microscopy, Rutherford backscattering, and Brillouin spectroscopy. The x-ray results indicate the preferred orientation of Cu {111} planes parallel to the Si substrate surface without any directional orientation for Cu-implanted SiO_2/Si(100) and for Cu-implanted and annealed SiO_2/Si(100). In the latter case, transmission electron microscopy reveals the presence of spherical nanocrystallites with an average size of ~2.5 nm. Rutherford backscattering shows that these crystallites (and the Cu in the as-implanted film) are largely confined to depths of 0.4–1.2 μm below the film surface. Brillouin spectra contain peaks due to surface, film-guided and bulk acoustic modes. Surface (longitudinal) acoustic wave velocities for the implanted films were ~7% lower (~2% higher) than for unimplanted SiO_2/Si(100). Elastic constants were estimated from the acoustic wave velocities and film densities. C_{11} (C_{44}) for the implanted films was ~10% higher (lower) than that for the unimplanted film. The differences in acoustic velocities and elastic moduli are ascribed to implantation-induced compaction and/or the presence of Cu in the SiO_2 film. © *2007 American Institute of Physics*. [DOI: 10.1063/1.2437690]

I. INTRODUCTION

The SiO_2/Si film-substrate interface system is widely used in the microelectronics industry for the fabrication of Si-based integrated circuits. It also finds application in passive optoelectronic devices such as waveguides. On the contrary, the use of nanocrystalline and nanostructured materials in these fields is limited. A composite materials system that takes advantage of the mechanical robustness of the SiO_2/Si interface and the novel structure-properties (unique optical, electronic, and magnetic properties) of nanocrystals could therefore serve as the platform from which new devices and components are constructed.[1,2] For example, nonlinear optical effects produced by Cu nanocrystals implanted in SiO_2 have already been investigated for use in future devices using the technique of degenerative four wave mixing.[3] Before such devices are developed, however, it is crucial that these complex materials systems are adequately characterized. In this article we report on some new characterization measurements for Cu nanocrystals in SiO_2 films grown on Si(100).

II. EXPERIMENTAL DETAILS

SiO_2 layers of 2 μm thickness were grown by wet thermal oxidation of Si(100) substrates. The SiO_2 was then implanted with high-energy ^{63}Cu ions at liquid N_2 temperature in a vacuum $<10^{-7}$ Torr using a National Electrostatics Corporation 5 SDH-4 1.7 MV tandem ion implanter. A multiple energy (0.7, 0.9, 1.2, 1.5 MeV), multiple dose (2.1, 4.2, 5.2, 7.2×10^{16} cm^{-2}) implant sequence yielded a Cu atomic concentration of ~3.6 at. % at ~0.6–1.0 μm depth. Both an as-implanted sample and an annealed sample (650 °C/1 h in N_2 gas containing 5% H_2) were characterized in the present study and compared to an unimplanted SiO_2 standard. The Cu concentration in the implanted samples was probed by Rutherford backscattering spectroscopy (RBS) performed with 3.5 MeV normal incident He^{++} ions. Figure 1 shows RBS spectra prior to and after annealing (the ordinate has been converted to units of Cu concentration and, hence, the RBS Si edge is not shown). Comparing the two spectra, negligible Cu diffusion (or loss of material) is apparent upon annealing, consistent with previous reports.[4]

Structural characterization was performed by x-ray methods [x-ray diffraction (XRD), pole figures] and transmission electron microscopy (TEM). The XRD measurements were carried out using Cu $K\alpha$ radiation from a Rigaku D/Max 2200V-PC diffractometer operating at 40 kV/40 mA and configured for the Bragg–Bretano focusing geometry. In order to obtain sufficient signal intensity, the system slits (scatter, receiving, divergence) were fully opened and a collection time of 10 s/step (2θ step size=0.002°) was used. The

a)Electronic mail: tandrews@physics.mun.ca

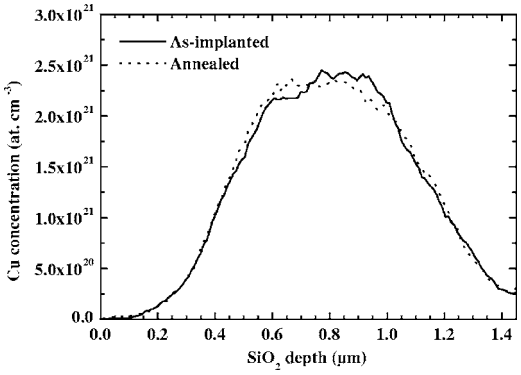

FIG. 1. Cu concentration versus depth for a Cu-implanted and a Cu-implanted and annealed 2-μm-thick SiO_2 film on a Si(100) substrate.

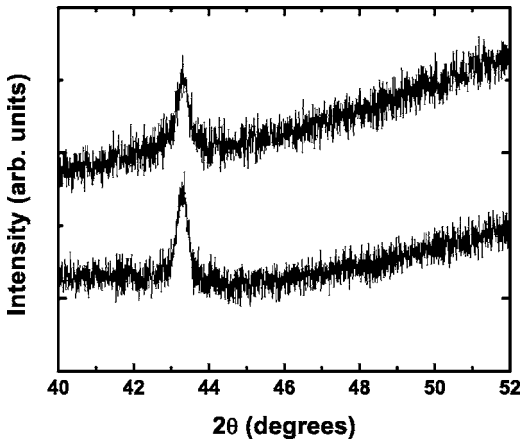

FIG. 2. X-ray diffraction spectra of a Cu-implanted (top) and a Cu-implanted and annealed (bottom) 2-μm-thick SiO_2 film on a Si(100) substrate.

(111) Cu and (111) Si pole figure measurements of the Cu phase and Si substrate were performed using the Schulz reflection method and multipurpose stage. For these measurements the 2θ angle of the Cu or Si phase is first fixed to the corresponding (111) plane of Cu or Si and x-ray scattering is detected as the sample inclination angle step increases every 2° for sample rotations varied between 0° and 360°.

TEM imaging was performed with a Philips CM300 electron microscope using an acceleration voltage of 300 kV. TEM samples were prepared in cross section and thinned by dual ion beam milling with 3 keV Ar ions at an angle of 5° from both sides until perforation.

Elastic characterization involved Brillouin light scattering studies that were carried out on the samples to determine acoustic wave velocities and elastic moduli. A single mode $Nd:YVO_4$ laser operating at a wavelength of 532 nm (p polarized) and a beam power of ~40 mW served as the incident light source. The scattered light was analyzed using a tandem (3+3)-pass Fabry–Pérot interferometer. In the case of a backscattering geometry, such as that used in these experiments, the bulk acoustic mode-induced frequency shift in the incident light is given by

$$f_B = \frac{2nV_B}{\lambda_i}, \tag{1}$$

where n is the refractive index of the material and λ_i is the wavelength of the incident light. V_B is either the transverse or longitudinal bulk acoustic wave (LAW) velocity, which, in the case of an isotropic material, are given by $V_T=\sqrt{C_{44}/\rho}$ and $V_L=\sqrt{C_{11}/\rho}$, respectively. C_{11} and C_{44} are elastic constants and ρ is the mass density. In the case of surface modes the frequency shift in the incident light is

$$f_R = \frac{2V_R \sin\theta_i}{\lambda_i}, \tag{2}$$

where V_R is the surface acoustic wave (SAW) velocity and θ_i is the angle of incidence.

III. RESULTS AND DISCUSSION

A. Structural characterization

XRD spectra (smoothed using the Savitzky–Golay method) for the as-implanted and implanted and annealed samples are presented in Fig. 2. There is one dominant peak that has been identified as the Cu (111) peak using a database provided by the International Center for Diffraction Data-Joint Committee on Powder Diffraction (Powder Diffraction File ICDD-JCPDS-PDF#4–836). The appearance of this peak in the spectra indicates that Cu crystallization has occurred in both the as-implanted sample and the implanted and annealed sample. This is clearly shown for the case of the latter sample in the high resolution cross-sectional TEM micrograph of Fig. 3(a) where it is evident that the Cu phase has precipitated into spherical Cu nanocrystals embedded in the amorphous SiO_2 film. Crystallization of Cu in the as-implanted sample was somewhat unexpected, but is not unprecedented for high dose (~10^{17} cm^{-2}) implantations.[4] It is also worth noting that the absence of peaks other than the Cu (111) peak in the XRD spectra [there is no Cu (200) peak, for instance, observed at the expected position of 2θ=50.6°] suggests that there is a preferred orientation for Cu in SiO_2 on Si(100).

Figure 3(b) shows the size distribution (obtained from cross-sectional TEM data) of the nanocrystals in the implanted and annealed sample. The nanocrystals have an average diameter of about 2.5 nm; such a nanocrystal is shown in the inset of Fig. 3(a). The reduced width of the Cu (111) peak in the XRD spectrum of the implanted and annealed sample relative to that in the spectrum collected from the as-implanted sample (see Fig. 2) indicates that these nanocrystallites are larger than those in the as-implanted sample. This is probably due to Ostwald ripening. As Fig. 1 shows, the nanocrystals are distributed over a depth range of about 0.4–1.2 μm below the sample surface.

X-ray pole figure measurements were carried out on the nanocrystalline Cu phase by (111) Cu pole figure and single crystal Si phase by (111) Si pole figure to see if there is any directional orientation in the recrystallized Cu phase as a consequence of growth or substrate influence. The results are shown as pole figure halves (111) Cu (top half) and (111) Si (bottom half) for the nanocrystalline Cu in SiO_2 on Si(100) samples as presented in Fig. 4. The Si pole figure half (bottom) shows poles corresponding to the (100) orientation of Si which has fourfold symmetry in Si(100). The Cu pole

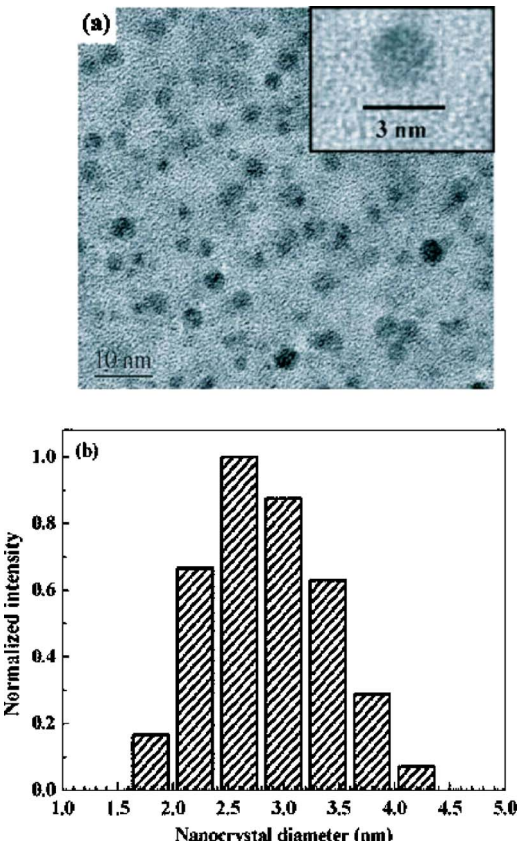

FIG. 3. (a) High resolution cross-sectional transmission electron microscopy micrograph of Cu nanocrystals in a Cu-implanted and annealed 2-μm-thick SiO_2 film on a Si(100) substrate. The inset shows an average-size crystallite with diameter ~2.5 nm. (b) Nanocrystallite size distribution obtained from the film described in (a).

figure half (top) has an increase in intensity in the pole figure center at 0° inclination and a weak outer ring at about 70°. These results indicate that a weak (111) fiber texture or preferred orientation without directional orientation exists for the nanocrystalline Cu phase in SiO_2 on Si(100).

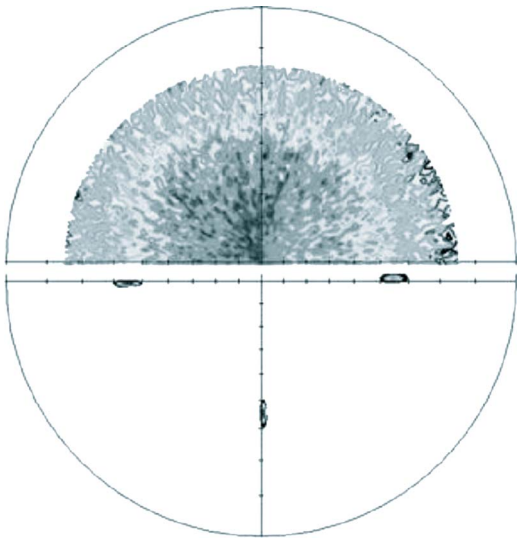

FIG. 4. X-ray diffraction pole figures of (111) Cu (top half) and (111) Si (bottom half) obtained from a Cu-implanted and annealed 2-μm-thick SiO_2 film on a Si(100) substrate.

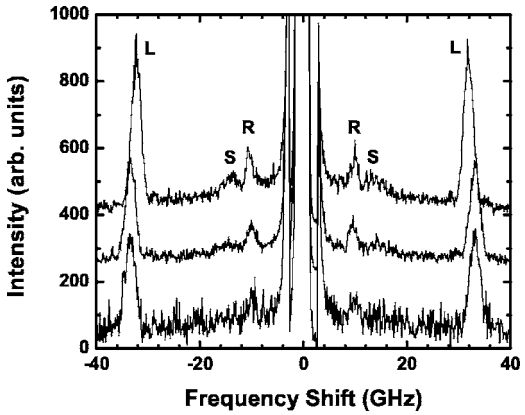

FIG. 5. Brillouin spectra collected at an angle of incidence $\theta_i=50°$ for an unimplanted (top trace), a Cu-implanted (middle trace), and a Cu-implanted and annealed (bottom trace) 2-μm-thick SiO_2 film on a Si(100) substrate. *R*, *S*, and *L* stand for the Rayleigh, Sezawa, and longitudinal modes, respectively.

Inspection of the micrograph of Fig. 3(a) and its inset shows that the Cu-SiO_2 interphase boundary displays no faceting and is accommodative to the stress field between the two phases. The nanocrystalline Cu phase appears to be free of line defects (such as dislocations) even at the boundary with the SiO_2 where one might expect to see microstructural defects in the case of a crystalline metal in contact with an amorphous solid. This suggests that the {111} preferred orientation of the nanocrystalline Cu phase is one of low interfacial energy. Similar results have also been observed for microcrystalline and nanocrystalline face-centered-cubic (fcc) metals such as Cu on SiO_2.[5,6] The {111} and {100} planes in fcc metals are the first and second most close-packed planes. They are commonly observed in thin film and single crystal studies of fcc metals on SiO_2 and Si. They have been described as preferred orientations that are the result of low surface and interfacial energy and also because of their ability to accommodate the effects of stress, with the {111} orientation several times more accommodative in terms of modulus than the {100} orientation for Cu on Si_3N_4 on Si, Cu on Si, Au, and Au-Cu embedded in SiO_2.[7–10]

B. Elastic characterization

Typical Brillouin spectra collected from the unimplanted, Cu-implanted, and Cu-implanted and annealed samples are presented in Fig. 5. The frequency shift of the peak labeled *L* (~±32 GHz) is independent of angle of incidence which suggests that it is due to a bulk acoustic mode [see Eqs. (1) and (2)]. Furthermore, its position in the spectra lies above the longitudinal threshold frequency for SiO_2 and is essentially the same as that of the longitudinal bulk acoustic mode of thermal oxide [as determined using Eq. (1) with the refractive index of thermal oxide provided by Ref. 11 and the density and elastic constant C_{11} as given in Ref. 12]. Moreover, peaks due to longitudinal bulk acoustic waves have been observed at approximately the same shift in backscattering spectra collected from silicate glass films with thicknesses on the order of 1 μm.[12,13] For the earlier reasons, and the fact that the film thickness is much larger than the acoustic wavelength (a few hundred nanometers), the *L* peak

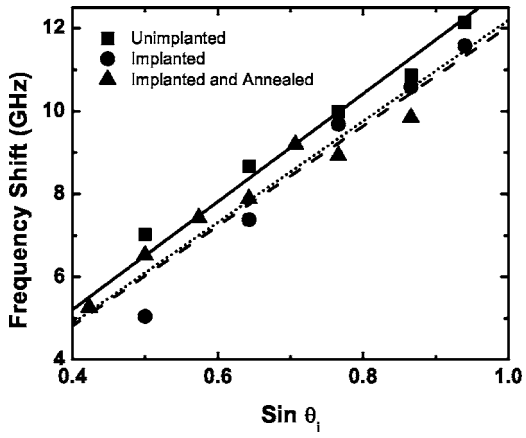

FIG. 6. Brillouin frequency shift vs sin θ_i for the Rayleigh mode for an unimplanted, a Cu-implanted, and a Cu-implanted and annealed 2-μm-thick SiO_2 film on a Si(100) substrate. The solid, dashed, and dotted lines are lines of best fit to the data obtained from the unimplanted, Cu-implanted, and Cu-implanted and annealed samples, respectively.

is assigned to the longitudinal acoustic bulk mode of the SiO_2 film. The peak labeled *R* has a frequency shift that varies linearly with sin θ_i and, for a given angle of incidence, has a shift that is lower than that of the transverse threshold frequency for SiO_2.[14] Thus it must be due to the Rayleigh surface mode propagating on the surface of the SiO_2 film. This mode has already been observed in Brillouin studies of supported SiO_2 films.[12,13,15,16] In order to accurately determine their Brillouin frequency shifts, Lorentzian functions were fit to the *L* and *R* peaks. The weaker feature at a shift intermediate to those of the *R* and *L* peaks is believed to be due to a Sezawa localized mode(s) (*S*). It has a frequency that varies linearly with sin θ_i. Sezawa modes have also been observed in previous Brillouin scattering experiments on the SiO_2/Si system.[12,15,16]

It is noted here that the Brillouin spectrum of a film/substrate system can contain peaks due to modes that propagate along the film-substrate interface (Stoneley waves). For two isotropic solids in contact with one another, the conditions imposed upon the elastic parameters for the existence of such waves are quite restrictive but well defined.[17] In the case of isotropic films on anisotropic substrates, little work has been done and thus the conditions for the existence of Stoneley waves in many such systems (e.g., the present case of SiO_2/crystalline Si) have not yet been established. Previous Brillouin studies[12,13,15] carried out on the SiO_2/crystalline Si system, however, make no mention of Stoneley waves. It is re-emphasized that the two spectral peaks that are the primary focus of the present work have been definitively assigned to the Rayleigh surface and longitudinal bulk acoustic modes of SiO_2 and thus are not due to Stoneley waves.

Figure 6 is a plot of Rayleigh mode frequency shift versus sin θ_i for the three samples. For a given angle of incidence, the frequency shift of the peak for the unimplanted sample is higher than that for the Cu-implanted and Cu-implanted and annealed samples. The Rayleigh SAW velocity for each of the three samples, obtained by linear least-squares fitting Eq. (2) to the data of Fig. 6, is presented in Table I. As is evident, the SAW velocity in both the Cu-implanted and Cu-implanted and annealed samples is about 7% lower than that in the unimplanted sample. This is probably due to implantation-induced compaction of the SiO_2 layer.[18,19] More specifically, the SAW velocity is given by $V_R \sim \sqrt{C/\rho}$, where *C* is an elastic constant and ρ is the density of the SiO_2 layer, and thus a decrease in the ratio C/ρ via implantation-induced changes in *C* and/or ρ would result in a reduction in SAW velocity relative to the unimplanted sample. In fact, one of the consequences of compaction is an increased density, the magnitude of which can be estimated from the Lorentz–Lorenz relation if the refractive index of the implanted SiO_2 film is known. This will be discussed in further detail later. It is also noted here that the presence of Cu (in whatever form) likely contributes little to the observed reduction in SAW velocity because the SAW propagates on the top $\sim$0.5 μm of the SiO_2 layer and the implanted Cu and the Cu nanocrystals that form from it are largely confined to greater depths (0.4–1.2 μm as shown in Fig. 1). That is, the SAW velocity is not influenced very much by the Cu because it is too deeply buried.

The decrease in SAW velocity is of the same order of magnitude as that obtained in Brillouin scattering studies of Ge nanoclusters synthesized by ion implantation and annealing in 500 nm thick thermal SiO_2 films.[20] In that case, the samples were doubly implanted with Ge^+ ions at energies of 450 keV (fluence of 3×10^{16} cm^{-2}) and 230 keV (fluence of 1.8×10^{16} cm^{-2}) at room temperature and annealed at 500 °C and again at 1100 °C in a dry N_2 ambient. These implantation parameters (energies and doses) most likely result in some compaction of the SiO_2 host but most of this is probably recovered upon annealing at 1100 °C. In any case (SAW velocity data is provided for the samples post-500 and post-1100 °C), the nanoclusters are located within the SAW prob-

TABLE I. Surface and longitudinal acoustic wave velocity, change in surface and longitudinal acoustic wave velocity relative to the unimplanted state, and approximate elastic moduli for an unimplanted, a Cu-implanted, and a Cu-implanted and annealed 2 μm-thick SiO_2 film on a Si(100) substrate.

Implanted species	Anneal temperature (°C)	SAW velocity (m/s)	Relative change in SAW velocity (%)	LAW velocity (m/s)	Relative change in LAW velocity (%)	C_{11} (GPa)	$C_{44}=G$ (GPa)	B (GPa)
Unimplanted		3470	···	5850	···	75.4	31.3	33.7
Cu	No Anneal	3210	−7.5	5950	1.8	82.3	28.2	44.8
Cu	650	3240	−6.4	5950	1.7	82.2	28.9	43.7

ing depth and, hence, may influence its velocity. It is therefore not possible to make quantitative comparisons with the results of the present study.

As alluded to earlier, and as shown in Table I, the SAW velocities for the as-implanted and the implanted and annealed samples differ by only ~1%. This similarity in the two velocities is attributed to the fact that the implantation-induced damage/compaction is only partially recovered by annealing at 650 °C/1 h. Support for this hypothesis is provided by Ref. 21 where profilometer measurements showed that the step height across the unimplanted/implanted boundary of Si-implanted fused silica were reduced, but not eliminated, upon annealing at 700 °C. The observation that the SAW velocity of the annealed sample is slightly higher than that of the as-implanted sample is also consistent with an incomplete recovery upon annealing at 650 °C for 1 h, although it is not clear if this slight difference is meaningful since it is within the estimated experimental uncertainty of ~2%. Near complete recovery of the compaction occurs at an anneal temperature of ~1000 °C.[21]

As for the SAW (i.e., R) peaks, the spectra presented in Fig. 5 reveal that the L peak frequency shifts for the as-implanted sample and the implanted and annealed sample are nearly equal (average shifts of 33.33 and 33.30 GHz, respectively). This represents an increase of about 4% relative to unimplanted SiO_2. In this case, because the LAW exists and propagates within the bulk of the film, this increase is ascribed to implantation-induced compaction of the SiO_2 film and/or the presence of Cu. Accurate determination of the relative influence of each of these mechanisms, however, is not possible with the present data, but a few general statements can be made regarding the contribution of each to the increased shift. In particular, Eq. (1) shows that the frequency shift of the L peak is proportional to both n and V_L and hence an increase in the product nV_L would result in a larger shift. It is well known that the compaction-induced density increase results in an increase in the refractive index of the SiO_2 which, for implant conditions similar to those used in this work, is ~2%.[22] A concomitant increase in the LAW velocity, which is given by $V_L=\sqrt{C_{11}/\rho}$, is also possible via an increase in C_{11}/ρ. That is, the percentage increase in elastic constant C_{11} because of compaction or the presence of Cu may be greater than the percentage increase in density.

Using the refractive index of thermal SiO_2 ($n_u=1.46$),[11] the approximate compaction-induced increase in index given above (which gives an index of refraction for the as-implanted and the implanted and annealed samples of $n_i \simeq 1.02n_u=1.49$), and the measured Brillouin frequency shifts, it is possible to estimate the LAW velocities from Eq. (1). These values are presented in Table I along with the change in LAW velocity relative to the unimplanted sample. The LAW velocities for the implanted samples are about 2% higher than those of unimplanted SiO_2. It is stressed here that in estimating the LAW velocities of the implanted samples it has been assumed that (i) the increase in refractive index is due solely to compaction of the SiO_2 film [i.e., the presence of the Cu (in whatever form) does not influence the refractive index] and (ii) the as-implanted sample and the implanted and annealed sample have the same refractive index. These assumptions are not strictly valid, but the relatively low concentration of Cu in the SiO_2 matrix and the apparently small post-anneal reduction in the compaction of the SiO_2 film suggest that they result in a reasonably accurate approximation to the refractive index of the implanted samples. In addition, it is noted that the implanted samples are treated as homogeneous in the sense that the refractive index is assumed to be the same throughout the SiO_2 film. This is not the case, but such a simplification is necessary in order to facilitate estimation of the LAW velocities.

Knowledge of the LAW and SAW velocities and densities allows estimation of elastic constants C_{11} and C_{44} via the equations for V_L and V_T given in Sec. II and the relation $V_R=\beta V_T$ where $0.87 \leq \beta \leq 0.96$ (Ref. 23) (here, in estimating C_{44}, the average value of $\beta=0.92$ is used). The density of each of the samples may be determined from the Lorentz–Lorenz relation

$$\rho = K\frac{n^2-1}{n^2+2}, \tag{3}$$

where $K=8.0461$ for SiO_2.[24] For the unimplanted sample with $n=n_u=1.46$ one obtains $\rho_u=2200\ \mathrm{kg/m^3}$ which yields $C_{11}^u=75.4$ GPa and $C_{44}^u=31.3$ GPa.

The densities of the as-implanted sample and the implanted and annealed sample were taken to be the same and were estimated from the Lorentz-Lorenz relation with $n=n_i=1.49$ (i.e., a 2% increase in index relative to unimplanted thermal SiO_2 as suggested by previous work[22]). The resulting values for C_{11}^i and C_{44}^i are given in Table I. As can be seen, $C_{11}^i \simeq 1.1C_{11}^u$ while $C_{44}^i \simeq 0.9C_{44}^u$. This difference in elastic constants is a consequence of their relationship to film density and acoustic wave velocity (via the equations given in Sec. II), which are different for the unimplanted and implanted layers because of implantation-induced compaction effects and/or the presence of Cu. It should also be noted that the values of C_{44} are actually estimates for the near-surface region of the samples since they were determined from SAW data and, as discussed earlier, the SAW has a non-negligible amplitude only on the top ~0.5 μm of the film.

Finally, it is worth mentioning that elastic constants C_{11} and C_{44} are related to the material bulk (B) and shear (G) moduli through the equations $C_{44}=G$ and $C_{11}=B+\frac{4}{3}G$. As can be seen in Table I, the bulk moduli for the implanted samples are ~30% larger than that for the unimplanted sample. This increase is most likely due to the reduction in compressibility that results from implantation-induced sample compaction (the bulk modulus is the reciprocal of the compressibility).

IV. CONCLUSIONS

Cu-implanted thermal SiO_2 films on Si substrates (annealed and unannealed) were studied using x-ray methods, TEM, RBS and Brillouin light scattering spectroscopy and compared to an unimplanted SiO_2 standard. Structural measurements by x-ray diffraction (scans and pole figures) show the presence of a fiber texture or (111) preferred orientation without directional preference for the Cu phase. This pre-

ferred orientation exists for both ion-implanted Cu and ion-implanted and annealed Cu in $SiO_2/Si(100)$. The (111) preferred orientation corresponds to the most close-packed plane for a fcc metal in contact with an amorphous/crystalline composite system of $SiO_2/Si(100)$. In the case of the implanted and annealed film, TEM results reveal the presence of spherical Cu nanocrystallites with a characteristic size of ~ 2.5 nm. RBS measurements show that these nanocrystallites (and the Cu in the as-implanted film) are largely confined to depths of $0.4-1.2$ μm below the film surface.

Brillouin spectra collected from each of the three samples contain peaks due to Rayleigh surface, film-guided, and bulk acoustic modes. SAW velocities, determined from Rayleigh mode frequency shift data, for both the implanted and the implanted and annealed films were found to be about 7% lower than that for the unimplanted sample. In contrast, the LAW velocities for the implanted films were $\sim 2\%$ higher than that for the unimplanted film, due in part to the fact that the LAW peak frequency shift for the implanted films was $\sim 4\%$ higher than that for unimplanted $SiO_2/Si(100)$. The SAW and LAW velocities, along with the corresponding film densities, permitted estimation of the elastic constants of the films. C_{11} (C_{44}) for the implanted films was found to be about 10% higher (lower) than that for the unimplanted film. The differences in acoustic wave velocities and elastic moduli for the implanted and unimplanted films are attributed to implantation-induced compaction effects and/or the presence of Cu in the SiO_2 film.

ACKNOWLEDGMENTS

B.J. and M.C.R. are grateful for financial support from the Australian Synchrotron Research Program, funded by the Commonwealth of Australia. M.C.R. would also like to thank the Australian Research Council for their financial support. The financial support of the Natural Sciences and Engineering Research Council of Canada (NSERC) is gratefully acknowledged by G.T.A. and J.S.

[1] Z. Liu, C. Lee, V. Narayanan, G. Pei, and E. C. Kan, IEEE Trans. Electron Devices **49**, 1606 (2002).
[2] A. Meldrum, L. A. Boatner, and C. W. White, Nucl. Instrum. Methods Phys. Res. B **178**, 7 (2001).
[3] L. Chae, M. Lee, H. K. Kim, and D. W. Moon, Bull. Korean Chem. Soc. **18**, 886 (1997).
[4] B. Johannessen, P. Kluth, C. J. Glover, G. de M. Azevedo, D. J. Llewellyn, G. J. Foran, and M. C. Ridgway, J. Appl. Phys. **98**, 024307 (2005).
[5] J. W. Sprenger, J. Shirokoff, and U. Erb, Scr. Metall. **23**, 1531 (1989).
[6] K. McCafferty, A. Soper, C. Cheung, J. Shirokoff, and U. Erb, Scr. Metall. Mater. **26**, 1215 (1992).
[7] S. P. Baker, A. Kretschmann, and E. Arzt, Acta Mater. **49**, 2145 (2001).
[8] J. N. Florando and W. D. Nix, Mater. Res. Soc. Symp. Proc. **673**, 1.9.1 (2001).
[9] G. De and C. N. R. Rao, J. Phys. Chem. B **107**, 13597 (2003).
[10] J.-M. Zhang, F. Ma, and K.-W. Xu, Appl. Surf. Sci. **229**, 34 (2004).
[11] A. Fargeix and G. Ghibaudo, J. Phys. D **17**, 2331 (1984).
[12] G. Carlotti, P. Colpani, D. Piccolo, S. Santucci, V. Senez, G. Socino, and L. Verdini, Thin Solid Films **414**, 99 (2002).
[13] G. Carlotti, L. Doucet, and M. Dupeux, Thin Solid Films **296**, 102 (1997).
[14] G. W. Farnell and E. L. Adler, *Physical Acoustics* (Academic, New York, 1972), pp. 35–127.
[15] V. Bortolani, F. Nizzoli, G. Santoro, and J. Sandercock, Phys. Rev. B **25**, 3442 (1982).
[16] V. Bortolani, A. M. Marvin, F. Nizzoli, and G. Santoro, J. Phys. C **16**, 1757 (1983).
[17] J. G. Scholte Mon. Not. R. Astron. Soc. **5**, 120 (1947).
[18] C. M. Johnson, M. C. Ridgway, A. Kurver, P. W. Leech, and P. J. Simpson, Nucl. Instrum. Methods Phys. Res. B **141**, 670 (1998).
[19] C. M. Johnson, T. D. Thompson, M. C. Ridgway, and V. Gurarie, Nucl. Instrum. Methods Phys. Res. B **141**, 629 (1998).
[20] J. Żuk, H. Krzyżanowska, M. J. Clouter, M. Bromberek, H. Bubert, L. Rebohle, and W. Skorupa, J. Appl. Phys. **96**, 4952 (2004).
[21] C. M. Johnson, M. C. Ridgway, and P. Leech, Appl. Phys. Lett. **69**, 984 (1996).
[22] P. D. Townsend, Rep. Prog. Phys. **50**, 501 (1987).
[23] G. W. Farnell, *Acoustic Surface Waves* (Springer, Berlin, 1978), pp. 13–59.
[24] E. A. Irene, E. Tierney, and J. Angillelo, J. Electrochem. Soc. **129**, 2594 (1982).